Poly(3,4-alkylenedioxypyrrole)s: Highly Stable Electronically Conducting and Electrochromic Polymers

Philippe Schottland, Kyukwan Zong, Carleton L. Gaupp, Barry C. Thompson, Christopher A. Thomas, Irina Giurgiu, Roberta Hickman, Khalil A. Abboud, and John R. Reynolds*

Department of Chemistry, Center for Macromolecular Science and Engineering, University of Florida, Gainesville, Florida 32611-7200

Received March 20, 2000; Revised Manuscript Received June 20, 2000

ABSTRACT: A series of poly(3,4-alkylenedioxypyrrole)s are reported as a new class of electronically conducting polymers exhibiting especially low oxidation potentials from ca. −0.6 to −0.4 V vs Fc/Fc^+ (equivalent to −0.15 to +0.05 V vs SCE) as desired for ambient stability of the doped and conducting states. These polymers exhibit unique combinations of multicolor electrochromism, switching from a red or orange neutral state to a light blue/gray doped state, passing through a darker intermediate state (brown), as examined by in situ colorimetry. High spectral contrast ratios have been measured throughout the visible region with a maximum $\Delta\%T = 76\%$ at 534 nm for poly[3,4-(2,2-dimethylpropylenedioxy)-pyrrole) (PProDOP−$(CH_3)_2$). PProDOP−$(CH_3)_2$ exhibits outstanding redox switching stability, being able to undergo 40 000 deep double-potential switches between its doped and neutral states (1 s, $\Delta\%T_{max} = 76\%$) while retaining more than 90% of its electroactivity. A high level of stability to overoxidation has also been observed as these materials show limited degradation of their electroactivity at potentials 2 V above their half-wave potential. Triflate-doped free-standing films of PEDOP and PProDOP, having high electrical conductivities of 83 and 95 S/cm, respectively, have been obtained by galvanostatic deposition at low temperature (−7 °C).

Introduction

Since the discovery of electrochromism,[1] electrochromic materials have aroused a great deal of interest in both academia and industry over the past 30 years.[2] In these materials, electrochemical oxidation and/or reduction gives rise to a reversible and visible change in reflected or transmitted light. These properties have proved especially promising for the construction of switchable mirrors,[3] displays,[4,5] windows,[6−10] and earth-tone chameleon materials.[11−13] For example, the recent commercialization of electrochromic rearview[14] and exterior wing automotive mirrors has been made possible by the development of highly stable electrochromic gels.[15]

The most extensively studied thin-film electrochromic materials are based on inorganic systems such as tungsten trioxide (WO_3) and iridium dioxide (IrO_2).[16] However, since many organic materials have redox-state-dependent electronic spectra, they undergo electrochemically driven color changes. Numerous classes of organic materials have proven interesting for electrochromics including viologens, metallophthalocyanines, and electroactive conducting polymers.[17] Among the organic materials, the use of conducting polymers is rapidly increasing[18] due to their ability to form durable films and because their optical properties can be tuned through molecular architecture.[19] In their neutral form, the extended delocalization of the π electrons along the polymer backbone results in an optical absorption band ($\pi-\pi^*$ transition) in the visible region of the electromagnetic spectrum. Upon doping, charge carriers are formed in the conjugated backbone, accompanied by the insertion of counterions, to balance the charge in the polymer. This process is referred to as p- or n-doping, depending on the nature of the redox process (oxidation or reduction), and results in the insertion of anionic or cationic dopant ions. An important asset of conducting polymers as electrochromic materials when compared to inorganic electrochromics is their outstanding coloration efficiency. As an illustration, poly(3,4-ethylenedioxythiophene) (PEDOT) derivatives can exhibit an order of magnitude larger change in coloration (optical density) when the same amount of charge is injected than for the widely used amorphous tungsten trioxide.[20] PEDOT derivatives are also remarkable for their fast switching ability as $\Delta\%T$ values of up to 70% can be attained with subsecond switching times.[21]

Here we report the synthesis and electrochromic properties of a new series of conjugated polymers which exhibit outstanding electrochromic properties: the poly(3,4-alkylenedioxypyrrole)s (PXDOPs). These polymers are among the lowest in oxidation potential for p-type doping ever reported ($E_{1/2}$ less than −0.6 V vs Fc/Fc^+). As a comparison, other conducting polymers such as poly(3-alkylthiophene)s (+0.3 to +0.5 V vs Fc/Fc^+),[22] polypyrrole (−0.5 to −0.3 V vs Fc/Fc^+),[23] and PEDOT (−0.4 to −0.2 V vs Fc/Fc^+) are more difficult to oxidatively dope to their conducting form with redox potentials which are a function of the dopant ion, solvent, and supporting electrolyte used.[24] This new series of polymers has been tailored to combine the outstanding properties of PEDOT derivatives, including stability,[24] optical contrast,[25] and lower band gap, with the intrinsic properties of polypyrroles, specifically low oxidation potential and aqueous compatibility. Analogous to the PEDOT series (PXDOTs), the presence of the cyclic alkylenedioxy moiety on the 3- and 4-position of the pyrrole ring results in a lowering of the band gap stemming from a raising of the HOMO (highest occupied molecular orbital) level.[26−28] Furthermore, both the new monomers and polymers exhibit a lower oxidation

10.1021/ma000490f CCC: $19.00
Published on Web 08/25/2000

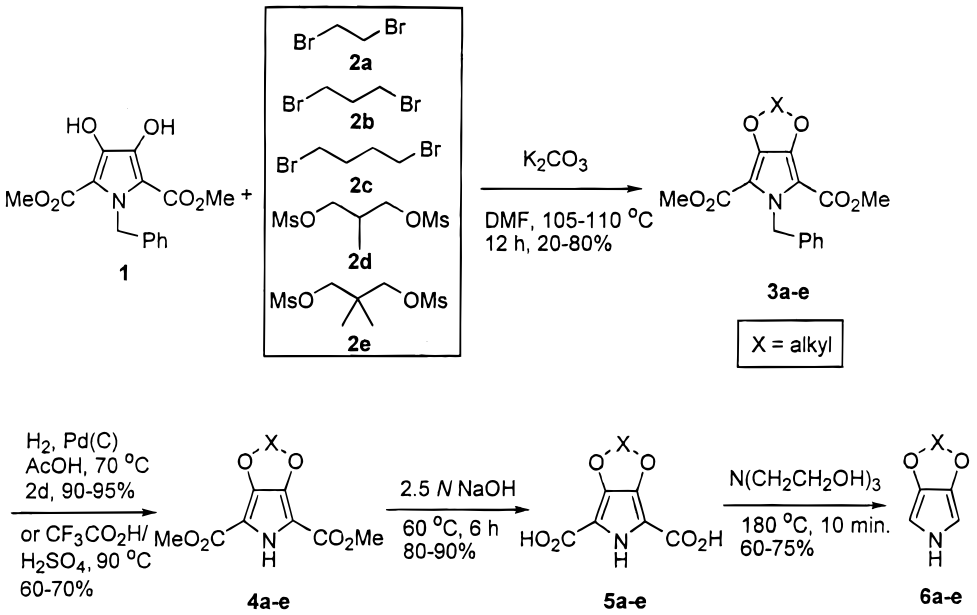

Figure 1. General reaction for the synthesis of 3,4-alkylenedioxypyrrole (XDOP) monomers.

potential than the pyrrole analogues, allowing a milder polymerization exclusively through the 2- and 5-positions which consequenty yields a regiosymmetric polymer with fewer structural defects.[29] The combined properties obtained in this new series of conducting polymers also allows them to be considered as potential biologically compatible materials.[30] As for their thiophene analogues (PXDOTs), these new electroactive polymers appear highly stable with a fast switching rate in organic electrolytes between the p-doped and neutral states. In addition, the PXDOPs offer a new dimension to electrochromics exhibiting multiple colors which makes them particularly interesting for display applications.

Results and Discussion

Monomer Syntheses. The 3,4-alkylenedioxy-substituted pyrroles (XDOPs) were prepared following the multistep procedure shown in Figure 1, which is similar to that employed for the 3,4-alkylenedioxythiophenes,[24,31,32] including additional protection/deprotection steps. Using a known procedure,[33] dimethyl-*N*-benzyliminodiacetate condenses with dimethyl oxalate under basic conditions to form dimethyl-3,4-dihydroxypyrrole-2,5-dicarboxylate (**1**) after acidification. The alkylenedioxy bridge on the pyrrole is then obtained by treating **1** with the corresponding dibromoalkanes or dimethanesulfonyl alkanes **2a**−**e** in the presence of potassium carbonate by refluxing the reaction mixture to afford **3a**−**e** in moderate to good yields. Debenzylation of compounds **3a**−**e** by catalytic hydrogenation, or via solvolysis, yielded **4a**−**e** which were then hydrolyzed in 2.5 M NaOH(aq) containing a small portion of ethanol to give diacids **5a**−**e** in good yields. Decarboxylation of the diacids **5a**−**e** was performed in triethanolamine at 180 °C. Purification of the crude materials by sublimation or recrystallization afforded the corresponding 3,4-alkylenedioxypyrrole derivatives **6a**−**e**. All monomers were subsequently handled under inert atmosphere as they are especially air-sensitive.

Structural Analyses. Single crystals of 3,4-ethylenedioxypyrrole (EDOP), 3,4-propylenedioxypyrrole (ProDOP), and 3,4-butylenedioxypyrrole (BuDOP) were obtained, and their crystal structures are determined as shown in Figure 2. The crystallographic parameters for these structures are listed in Table 1. Note that EDOP crystallizes in a monoclinic system whereas ProDOP and BuDOP are orthorhombic. A slight difference in density is observed with EDOP at 1.384 g/cm^3, ProDOP at 1.405 g/cm^3, and BuDOP at 1.302 g/cm^3. The 3,4-oxygen atoms lie within 2° of the pyrrole ring in the case of EDOP and ProDOP and within 7° for BuDOP. It should be noted that the pyrrole ring in BuDOP and EDOP is more planar than in ProDOP with a torsion angle C1−N1−C4−C3 of 0.2°, 0.4°, and 1.1° for EDOP, ProDOP, and BuDOP, respectively. As expected, the alkoxy groups efficiently donate electrons to the π-system and increase the electron-rich character of both molecules. The major difference between the structures is the strain in the alkylenedioxy ring. In EDOP, the six-membered fused ring yields an O3−C6−C5 angle which is equal to 111.4° and close to ideal (109.47° for a sp^3 carbon) reflecting a low strain in the ring. This is further confirmed by the O3−C3−C2 angle (123.7°) which is also close to ideal (120°). In ProDOP, on the other hand, the O3−C3−C2 angle is 126.6°, and the carbon dihedral angles in the propylene bridge are 113.4° (O3−C7−C6) and 115.4° (C7−C6−C5). As a result of the induced ring strain, we can expect a slightly less effective π-overlap between the dioxy substituents and the ring, thus inducing a slight decrease in the electron density compared to EDOP. In BuDOP the O3−C3−C2 angle is further increased to 127.6°, and the carbon dihedral angles in the butylene bridge are 113.3° (O3−C8−C7), 116.1° (C8−C7−C6), and 115.5° (C5−C6−C7). It should be noted that the bond angle at the oxygen atom appended to the pyrrole (C3−O3−C6, C3−O3−C7, and C3−O3−C8), which reflects the strain in the alkylenedioxy bridge, increases with the size of the bridge with 109.4°, 114.3°, and 115.4° for EDOP, ProDOP, and BuDOP, respectively. The bond angle at the other oxygen atom appended to the pyrrole (C2−O2−C5) follows the same trend with 109.1°, 113.1°, and 116.1° for EDOP, ProDOP, and BuDOP, respectively. The strain induced by the butylene bridge in BuDOP should slightly reduce the electronic donating effect of

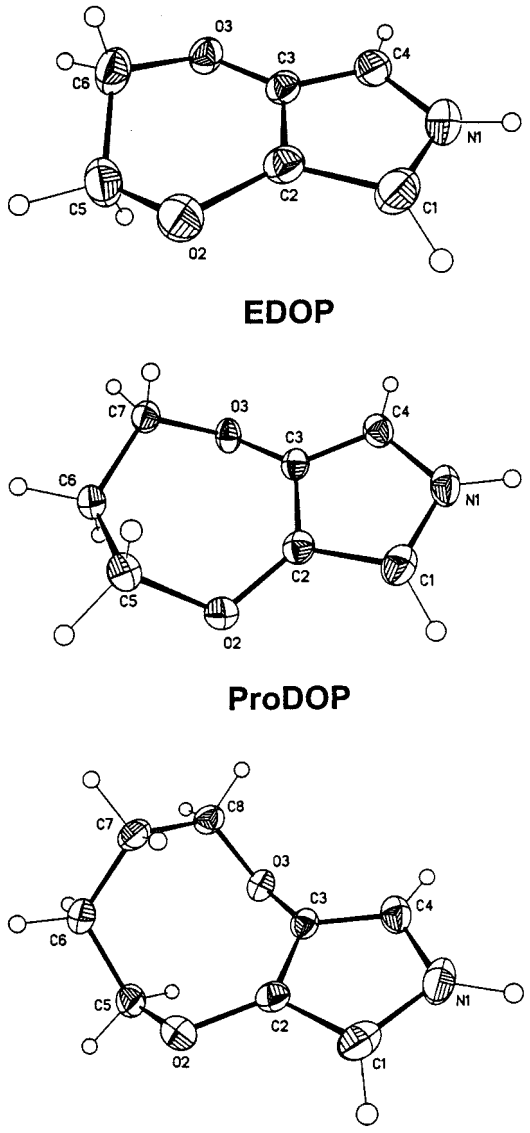

Figure 2. Perspective view and atom labeling of the crystal structure of EDOP, ProDOP, and BuDOP.

the 3,4-butylenedioxy substituent. On the other hand, the higher planarity of the pyrrole ring increases the electron density in the heterocyle and may compensate the effect of the strain. Slightly different electrochemical and optical properties are then expected for EDOP, ProDOP, and BuDOP as a result of the structural differences.

Electrochemical Polymerization. Oxidative electrochemical polymerization was carried out in propylene carbonate (PC) with 0.1 M $LiClO_4$ as electrolyte. The electrolyte choice was driven by the optimal results obtained for pyrrole electropolymerization in the same medium.[34] The peak oxidation potentials ($E_{p,m}$) obtained during the first scan at a bare Pt electrode for each of the monomers are summarized in Table 2. The potentials are found to vary over a relatively small 100 mV range, and all of the compounds electropolymerize quite efficiently. While these monomers oxidize at essentially the same potential, it is somewhat lower than that for pyrrole (+0.9 vs Fc/Fc^+), which can be attributed to the electron-rich character of the monomer and ease of formation of the radical cation at the electrode.

Table 1. Crystallographic Results for EDOP, ProDOP, and BuDOP

	EDOP	ProDOP	BuDOP
	Crystal Data (173 K)		
a, Å	8.580(1)	10.2041(7)	12.9483(7)
b, Å	6.7598(9)	10.2504(7)	9.1631(5)
c, Å	10.696(1)	12.5818(9)	13.1679(8)
α, deg	90.00	90.00	90.00
β, deg	104.460(3)	90.00	90.00
γ, deg	90.00	90.00	90.00
vol, Å^3	600.7(1)	1316.0(2)	1562.3(1)
d_{calc}, g cm^{-3}	1.384	1.405	1.302
empirical form	$C_6H_7NO_2$	$C_7H_9NO_2$	$C_8H_{11}NO_2$
formula wt, g	125.13	139.15	153.18
crystal system	monoclinic	orthorhombic	orthorhombic
space group	*P*2(1)/c	*Pbca*	*Pbca*
Z	4	8	8
F(000), electrons	264	592	656
crystal size, mm^3	0.30 × 0.25 × 0.10	0.28 × 0.27 × 0.07	0.28 × 0.21 × 0.08
	Data Collection (173 K)		
radiation, *λ* (Å)	Mo Kα, 0.710 73		
θ range, deg	2.45− 27.50°	3.24−27.49°	3.09−27.50°
range of *hkl*	$-4 \le h \le 11$	$-13 \le h \le 13$	$-16 \le h \le 16$
	$-8 \le k \le 4$	$-13 \le k \le 12$	$-11 \le k \le 9$
	$-13 \le l \le 12$	$-16 \le l \le 12$	$-17 \le l \le 16$
reflections coll	2442	8992	10 735
unique reflect	1313	1505	1789
abs coeff, mm^{-1}	0.105	0.104	0.094
max, min trans	0.9884, 0.9697	0.9934, 0.9755	0.9925, 0.9761
	Structure Refinement		
S, goodness of fit	1.011	1.038	1.041
reflections used	1313, $I > 2\sigma(I)$	1505, $I > 2\sigma(I)$	1789, $I > 2\sigma(I)$
no. of variables	83	91	101
R_1, wR_2 (%)	4.08, 10.15	3.80, 9.22	3.77, 10.11
R_{int} (%)	6.10	4.85	4.71
min peak in diff Four. map (e Å^{-3})	−0.175	−0.187	−0.183
max peak in diff Four. map (e Å^{-3})	0.213	0.220	0.299

Table 2. Oxidation Potentials, Band Gaps, and Optical Contrast Ratios between Doped and Neutral States of the PXDOPs

polymer	$E_{ox,m}$[a] (V)	$E_{1/2,p}$[a] (V)	E_g (eV)	λ_{max} (nm)	Δ(%*T*)[b]
PEDOP	0.73	−0.58	2.0	537	59
PProDOP	0.75	−0.50	2.2	522	70
PProDOP−CH_3	0.78	−0.49	2.2	530	51
PProDOP−$(CH_3)_2$	0.83	−0.37	2.2	534	76
PBuDOP	0.73	−0.55	2.2	533	61

[a] Potentials are reported vs Fc/Fc^+. [b] Optical contrast ratios are determined at λ_{max}.

Electropolymerization for all of the monomers was carried out using multiple scan cyclic voltammetry in 0.1 M $LiClO_4$/PC. The electrodeposition of PProDOP from a 10^{-2} M solution of monomer in the electrolyte is shown in Figure 3A and is illustrative for each system. The multiple cyclic voltammograms show the fast and regular growth of PProDOP at the platinum working electrode as evidenced by the redox process of the as-made polymer film.

To determine the relative polymerization efficiencies and film formation capabilities, the rates of potentiostatic electropolymerization with concurrent film growth

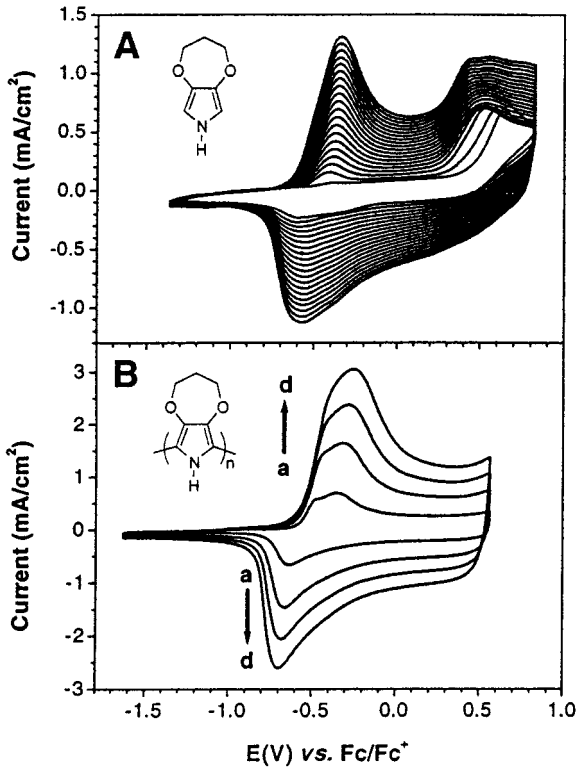

Figure 3. **(**A**)** Electrodeposition of PProDOP by potential scanning from a 10^{-2} M solution of ProDOP in 0.1 M $LiClO_4$/PC at 20 mV/s on a Pt button (area = 0.02 cm^2). **(**B**)** Cyclic voltammogram of PProDOP in 0.1 M $LiClO_4$/PC at a scan rate of (a) 20, (b) 50, (c) 75, and (d) 100 mV/s.

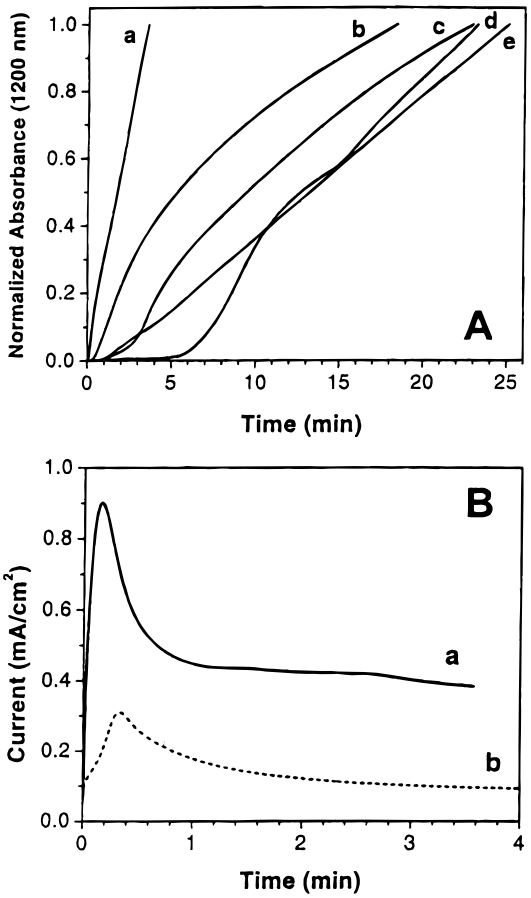

Figure 4. **(**A**)** Comparison of the growth rate of PXDOPs followed by NIR spectroscopy. Electrodepositions of a 100 mC/cm^2 film were performed from a 10^{-2} M solution of XDOP in 0.1 M $LiClO_4$/PC at a potential 50 mV higher than the monomer oxidation. Normalized absorbances at 1200 nm [Abs(t)/Abs(final)] are presented as a function of time for (a) PProDOP, (b) PEDOP, (c) PProDOP$-(CH_3)_2$, (d) PProDOP$-CH_3$, and (e) PBuDOP. **(**B**)** Evolution of the current density during potentiostatic deposition on a Pt button (diameter 0.02 cm^2) of (a) PProDOP at +0.80V vs Fc/Fc^+ and (b) PEDOP at +0.78 V vs Fc/Fc^+ from a 10^{-2} M solution of monomer in 0.1 M $LiClO_4$/PC.

were monitored for each monomer at an applied potential equal to the monomer peak potential ($E_{p,m}$) plus 50 mV on an ITO-coated glass substrate. The absorbance in the near-infrared (NIR) at 1200 nm due to charge-carrier absorption was recorded as a function of time until a charge of 100 mC/cm^2 was passed. The value of 1200 nm does not correspond to the maximum absorbance in the NIR region but is a useful value which can be used without saturating the detector. PProDOP exhibits the fastest deposition rate of the series, suggesting that the reactive intermediate radical cations couple quickly to form a macromolecular chain that deposits and continues to polymerize on the electrode surface without involving soluble oligomers. For the other polymers, a variable induction period ranging from a few seconds for EDOP to a few minutes is observed. We attribute this to the formation of soluble oxidized oligomers whose concentration builds up in solution before deposition and further polymerization on the electrode surface. PEDOP, PProDOP$-(CH_3)_2$, and PBuDOP display a similar growth rate after approximately 5 min of electropolymerization. The most pronounced results are seen for PProDOP$-CH_3$ which exhibits the longest induction period prior to onset of the NIR absorbance (see Figure 4A, curve d) followed by a period of rapid deposition. Further film deposition then occurs at a rate similar to the other polymers. These results are indicative of the complexity of the electropolymerization/concurrent deposition methodology where various processes control the electrodeposition rates.

Monitoring the current during these potentiostatic electrodepositions gives further information on the deposition mechanism, as illustrated in Figure 4B for PProDOP and PEDOP. In each case, the initial nucleation process is represented by the rapid increase in current during the first 10−20 s of the experiment. It should be noted that these current increases occur during times well beyond the double-layer charging of the electrode. The increase of the current is then limited by mass transport,[35] as illustrated by a current peak and a subsequent decrease in current response as the growth rate becomes diffusion limited. The lower currents observed during PEDOP deposition are expected, since it electropolymerizes at a rate slower than PProDOP. The current−time profiles observed for ProDOP$-CH_3$ and ProDOP$-(CH_3)_2$ electropolymerizations are more complex, due to the formation of the soluble oligomers before electrodeposition.

On the basis of these results, we have performed galvanostatic electrodepositions of the different polymers. Optimization of the current density to 0.05 mA/cm^2 yielded a stable electropolymerization potential and films that are extremely smooth (see below) and compact and could be removed from the electrodes.

Free-Standing Films. To properly prepare free-standing films for electrical property characaterization, it is important to understand the relationship between

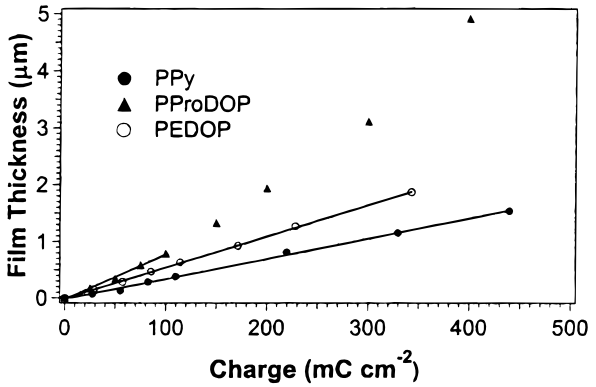

Figure 5. Comparison of film thickness as a function of charge density for PPy (●), PProDOP (▲), and PEDOP (○).

film thickness and deposition charge. Results obtained for PEDOP and PProDOP via profilometry support the electrochemical and spectroscopic results presented above. Figure 5 indicates the order of polymerization efficiency to be PProDOP > PEDOP > PPy. Because of the oxidation potential differences between the dioxypyrroles and pyrrole, it is not surprising that the DOPs polymerize more efficiently. Explaining the differences within the DOP family are complicated by numerous other factors including interactions of the monomers, reactive intermediates, and growing polymer chains with dopant ions and solvent. Furthermore, at a given charge density, PProDOP−OTs (OTs = $CH_3C_6H_4SO_3^-$) is over twice as thick as an identically prepared film of PPy−OTs. Density studies on galvanostatically deposited film for the parent polymers (PPy, PEDOP, PProDOP) indicate that they have similar densities of ca. 1.4−1.5 g cm^{-3}, which are comparable to other polypyrroles reported (ca. 1.3−1.6 g cm^{-3} depending on the identity of the dopant ion).[36]

Free-standing films of PProDOP, PEDOP, and PPy having the highest quality were prepared at reduced temperature. The dioxy-substituted monomers form powdery deposits at the temperatures (−40 to −20 °C) commonly used to grow PPy, but PProDOP and PEDOP form flexible films that are not prone to tearing at −7 °C. When prepared in the form of relatively thick (1−3 μm) free-standing, dark blue films, PProDOP−OTf (OTf = $CF_3SO_3^-$) exhibits a conductivity of 95 S/cm, as measured with a four-probe method.[37,38] PEDOP−OTf forms black films under these growth conditions with a conductivity of 83 S/cm. At even further reduced temperatures (−15 to −30 °C), PPy−OTf films exhibit conductivities as high as 250 S/cm. Films of comparably high conductivities and film properties are also obtained with tosylate (OTs)- and hexafluorophosphate (PF_6^-)-doped PProDOP, PEDOP, and PPy. Surface roughnesses determined by profilometry for films prepared on glassy carbon amounts to 4% on average.

Electrochemical and Spectroscopic Characterization. Polymer films were deposited on a platinum electrode by scanning the potential for 20 cycles between −1.30 V vs Fc/Fc^+ and the $E_{ox,m}$ plus 50 mV in PC using 0.01 M monomer and 0.1 M $LiClO_4$ as electrolyte. The samples were then characterized by cyclic voltammetry in monomer-free electrolyte. The scan rate dependence for the redox switching of PProDOP is shown in Figure 3B. The peak currents in the cyclic voltammograms increase linearly with the scan rate up to 100 mV/s, indicating that the electroactive sites are surface bound to the platinum working electrode and that the oxidation and reduction processes are not diffusion limited. The half-wave potentials ($E_{1/2,p}$) for each of the polymers are summarized in Table 2. It is noteworthy that these polymers exhibit extremely low $E_{1/2,p}$ values that are among the lowest reported, if not the lowest, for any conducting polymer family. This intrinsic property is of particular importance since it gives an indication of the stability of the polymer in the doped state. As previously reported by us,[30] such low oxidation potentials are a tremendous asset when compared to regular polypyrroles for biological applications as illustrated by the stability of doped PEDOP toward strong biological reductants.

Among the polymers studied here, PEDOP has the lowest $E_{1/2,p}$ of the series at −0.58 V vs Fc/Fc^+. In considering the ProDOP series, the more substituted the repeat unit, the higher the oxidation potential. Consequently, PProDOP−$(CH_3)_2$ is the most difficult to oxidize of the series with an $E_{1/2,p}$ of −0.37 V vs Fc/Fc^+, though it is still quite low relative to most conjugated polymers. The monomer BuDOP presented an oxidation potential almost identical to EDOP. This trend is also observed in the polymers since PBuDOP exhibits a half-wave potential value of −0.55 V vs Fc/Fc^+, which is very close to that of PEDOP. Such a low oxidation potential in the polymer may result from the higher planarity of the pyrrole ring in the BuDOP repeat unit, despite a higher strain in the alkylene bridge compared to other 3,4-alkylenedioxypyrrole monomers, as suggested by the crystal structure of the monomer.

The stability of the PXDOPs upon switching was investigated by exposing polymer films (about 1 μm in thickness) deposited by potential scanning on a platinum electrode, to repeated doping/dedoping processes involving at least 97% of the maximum charge as determined by the charge/time profile. The films were held for one second at each potential (−1.63 and +0.41 V vs Fc/Fc^+), and a cyclic voltammogram was recorded every 100 switches up to a total of 40 000 switches. The charge involved in the electrochemical process was calculated for each voltammogram, and the total charge lost during this experiment decreases by less than 10%. Consequently, the stability of the PXDOPs is outstanding since they retain more than 90% of their electroactivity, even after 40 000 switches.

In electrochromic devices, stability is of fundamental importance. Polypyrroles are known to be highly sensitive to overoxidation[39] where, at high potentials, reactions can occur in position 3 or 4 of the pyrrole ring, degrading the conjugated polymer backbone. The presence of a blocking substituent, such as the 3,4-alkylenedioxy bridge, avoids this type of degradation, and consequently, the polymer is stable to higher potentials. To illustrate this increase in the stability upon oxidation, we have exposed several films of PPy, poly(3,4-ethylenedioxythiophene) (PEDOT), and PProDOP to a series of potentials above the $E_{1/2,p}$ (from +0.75 to 3.0 V) for 2 min. After each high potential exposure, a cyclic voltammogram was then carried out by scanning at 20 mV/s between −1.63 and +0.38 V vs Fc/Fc^+. The relative electroactivity of each polymer film, measured as the ratio of the total charge involved in the redox process after high potential exposure, to the charge integrated from the cyclic voltammogram of the freshly prepared film, was then determined. The results, presented in Figure 6A, show the outstanding stability of PProDOP to overoxidation as only a slight decrease of the elec-

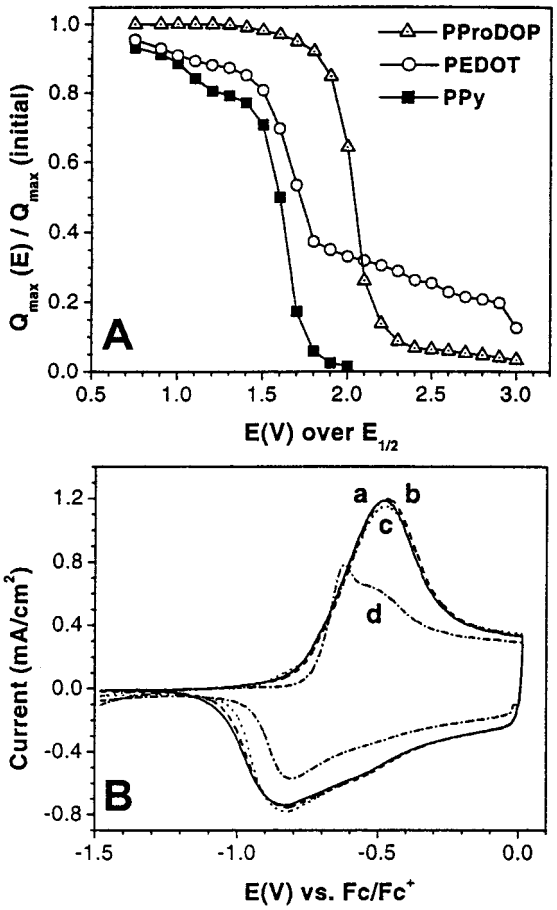

Figure 6. **(**A**)** Comparison of the stability to overoxidation for galvanostically deposited films (200 mC/cm^2) of PPy, PEDOT, and PProDOP. The relative electroactivity is defined as the ratio of the maximum charge stored in the polymer film after holding for 2 min at a potential over $E_{1/2}$ ($Q_{max}(E)$) to the charge initially stored in the as grown film (Q_{max}(initial)). **(**B**)** Cyclic voltammogram in 0.1 M $LiClO_4$/PC at a scan rate of 20 mV/s of a PProDOP film: (a) as grown, and after holding for 2 min at (b) +1.0, (c) +1.5, and (d) +2.0 V above $E_{1/2}$.

troactivity is noted when the holding potential was raised to about 2.0 V over $E_{1/2,p}$. At the same potential over $E_{1/2}$, no electroactivity is seen in PPy or PEDOT. While PEDOT is often referred as the most stable conducting polymer prepared to date, it is not as resistant as PProDOP to overoxidation. Figure 6B shows the evolution of the cyclic voltammogram for PProDOP after exposure to potentials over $E_{1/2,p}$. It is evident that there is no change in the cyclic voltammogram up to +1.5 V over $E_{1/2,p}$. Even at 2.0 V over $E_{1/2,p}$ (Figure 6B, curve d), the cyclic voltammogram of PProDOP still displays a clear redox process, suggesting that, while some of the electroactive sites have been destroyed, the polymer film is still quite electroactive. It should be noted that the electroactivity of PEDOP exhibits a comparable stability to that of PProDOP. However, the degradation mechanism seems to be quite different in PEDOP because the redox process is shifted to higher potentials when the holding potential is increased, though only a limited decrease of the electroactivity is observed. This behavior may be explained by the creation of defects (conjugation breaks) in the conjugated backbone which result in the formation of segments with a shorter conjugation length, and therefore a higher half-wave oxidation potential, which still retain a high degree of electroactivity.

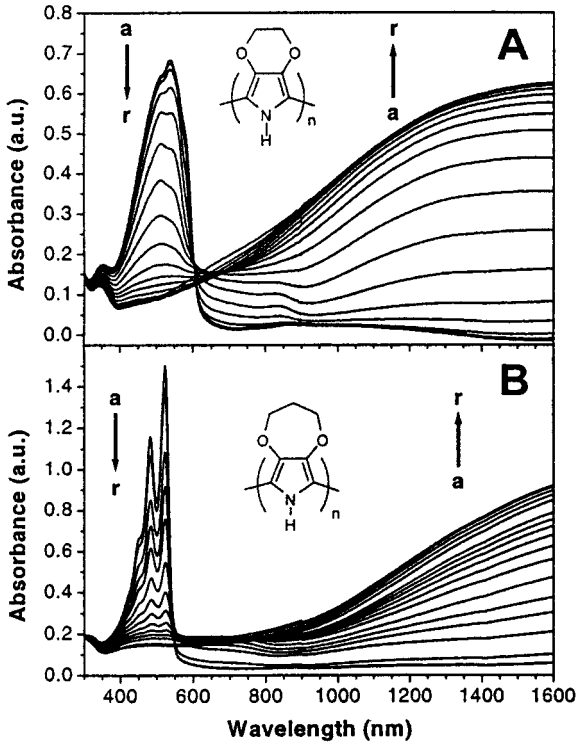

Figure 7. **(**A**)** Spectroelectrochemistry of PEDOP in 0.1 M $LiClO_4$/PC at applied potentials of (a) −1.33, (b) −1.23, (c) −1.13, (d) −1.03, (e) −0.98, (f) −0.93, (g) −0.88, (h) −0.83, (i) −0.78, (j) −0.73, (k) −0.68, (l) −0.63, (m) −0.53, (n) −0.43, (o) −0.33, (p) −0.23, (q) −0.13, and (r) +0.07 V vs Fc/Fc$^+$. **(**B**)** Spectroelectrochemistry of PProDOP in 0.1 M $LiClO_4$/PC at applied potentials of (a) −1.13, (b) −1.03, (c) −0.93, (d) −0.88, (e) −0.83, (f) −0.73, (g) −0.62, (h) −0.58, (i) −0.53, (j) −0.48, (k) −0.43, (l) −0.38, (m) −0.33, (n) −0.23, (o) −0.13, (p) −0.03, (q) +0.07, and (r) +0.17 V vs Fc/Fc$^+$.

Spectroelectrochemical Analysis. The optical properties of the PXDOPs were examined by spectroelectrochemistry, as illustrated by the results in Figure 7. It is immediately obvious that the absorption bands seen for the PXDOPs are well defined, contrasting with the broad bands generally observed in regular polypyrrole.[40] Two types of behavior were found which differ only by the shape of the $\pi-\pi^*$ absorption band in the neutral state. In PEDOP, the $\pi-\pi^*$ transition absorbs at a λ_{max} of 537 nm, and no (or very little) vibronic coupling is observed (see Figure 7A). This is in contrast to the other PXDOPs, as exemplified by PProDOP in Figure 7B. As a result of vibronic coupling, the electronic spectrum of PProDOP (Figure 7B) shows a split of the $\pi-\pi^*$ transition with a shoulder at 450 nm and two maxima at 482 and 523 nm. This behavior, which is often seen in the PXDOTs,[21] suggests a higher degree of regularity[41] in PProDOP relative to PEDOP, possibly due to preferential trans orientation of the PProDOP rings relative to one another. This trend is not surprising since the characterization of PEDOP by cyclic voltammetry shows broader oxidation and reduction peaks than PProDOP.

The electronic band gaps (taken as the onset of the $\pi-\pi^*$ transition) are summarized in Table 2 and found to be quite well-defined. Comparing these polymers, PEDOP is the exception with a band gap of 2.0 eV, whereas a band gap of 2.2 eV is found for the other PXDOPs. Several energetic contributions control the value of the band gap.[42] These include the energy related to bond length alternation, the mean deviation from planarity, aromatic resonance energy, the induc-

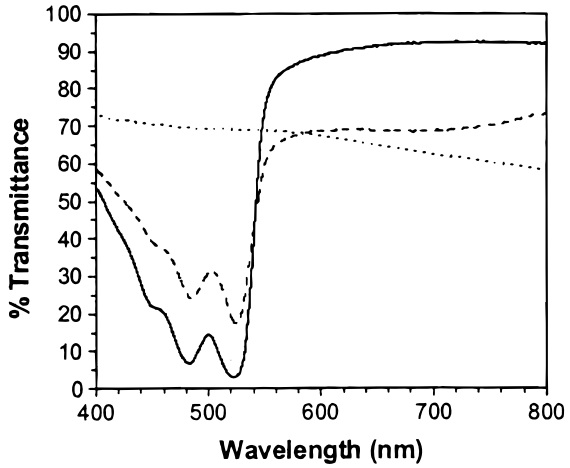

Figure 8. Transmittance of PProDOP in the visible region as a function of wavelength (nm) for three different oxidation states: neutral (solid line), intermediate (dashed line), and fully oxidized (dotted line).

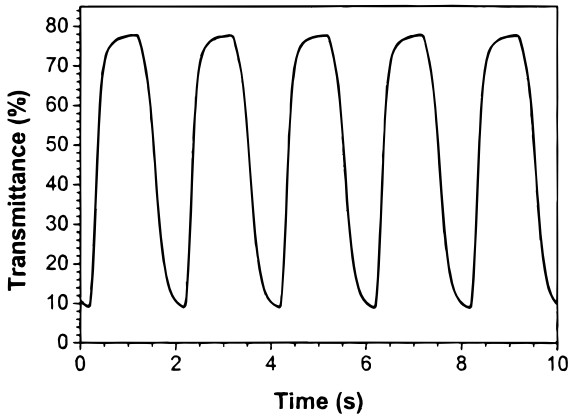

Figure 9. Variation of transmittance for PProDOP as a function of time for the first five switches (step time: 1 s) between −1.13 and +0.17 V vs Fc/Fc^+ in 0.1 M $LiClO_4$/PC.

tive or mesomeric electronic effects of substituents, and interchain coupling in the solid state. Usually, the quinoid form has a smaller band gap because, in the quinoid form, exocyclic double bonds force planarity between adjacent rings.[43] A longer alkylenedioxy chain induces a larger strain, and therefore the quinoid form is less favorable as the rings are twisted from planarity. Thus, the lowest band gap is found in PEDOP. For PBuDOP and PProDOP, as well as its substituted derivatives, the deviation from planarity is similarly mirrored by the identical band gaps.

As illustrated in Figure 7, the $\pi-\pi^*$ transition decreases upon oxidation with the concurrent formation of a broad band located in the near-infrared (NIR). This low-energy absorption is associated with the charge carriers (radical cation and dication) formed in the doped polymers. Note that the NIR absorption of doped PEDOP (Figure 7A, curve r) tails into the visible region of light, while in the other PXDOPs, as exemplified by PProDOP (Figure 7B, curve r), the NIR band is red-shifted and allows a higher degree of light transmission over the visible region. The transmittance spectra of a thin film (about 0.1 μm) of PProDOP, in both neutral and doped states, is presented in Figure 8. The deep orange-red color is evident in the neutral form, as is the color neutrality of the doped form as only a flat transmittance spectrum is observed. By controlling the thickness of the films, it is thus possible to easily control the optical density of these highly transmissive conducting films. Interestingly, a brown intermediate doped state to be discussed further below is observed, and the measured transmittance is also reported in Figure 8. The optical contrasts, measured at λ_{max} for the PXDOPs, are presented in Table 2 for 0.1 μm thick films. We observe $\Delta\%T$ to vary between 51 and 76% for the different polymers studied. Note that PEDOP exhibits a lower contrast ratio (59%) than PProDOP (70%) due to the tail of the broad NIR absorption of the doped state. The intermediate state is characterized by an increased transmittance in the $\pi-\pi^*$ region but a decreased transmittance at longer wavelengths stemming from the onset of the absorbance of the charge carriers in the NIR.

Electrochromism and Colorimetry. An important aspect of redox active conducting polymers as materials potentially useful for electrochromic displays is their ability to switch rapidly from one state to another. This ability has already been demonstrated in the PXDOT family of materials as these polymers switch in less than 1 s with high contrast ratios in the visible region of the spectrum.[21] The PXDOPs, as well as their thiophene analogues, are also able to switch between their neutral and doped states in less than 1 s with high contrast ratios. In these experiments, we have chosen the switching times as the times required to switch 95% of the maximum contrast at the wavelength of the maximum absorption. This behavior is illustrated in Figure 9 for PProDOP when switched between −1.32 and +0.18 V vs Fc/Fc^+, which requires less than 200 ms to switch. All of the PXDOPs show an excellent stability of their electrochromic properties and are able to switch (deep double potential switching) between their fully doped and neutral states thousands of times with limited degradation.

Coloration efficiency[2] provides information about the contrast ratio obtained for a certain charge injected in the material, making it a figure of merit for electrochromic materials. In general, organic electrochromic compounds are more efficient than typical inorganic materials.[2] Conjugated polymers, and more particularly the PXDOTs, exhibit fairly high coloration efficiencies which allow the construction of dual polymer devices with a coloration efficiency above 1000 cm^2/C. The coloration efficiencies of the PXDOPs were measured at the maximum absorption of the $\pi-\pi^*$ transition. Again, relatively high values are measured (about 600 cm^2/C) which indicates that the PXDOPs give a high contrast with a very thin layer of polymer. Note that while the coloration efficiency is a useful parameter for materials that switch between a highly colored and a colorless state, the results are obtained at a single wavelength. The use of coloration efficiencies in comparing materials that change from one color state to another is not especially meaningful.

When considering an electrochromic material for use in particular applications, the color of the material is obviously important, and a precise definition of color is required. We have studied the polymers by colorimetry and express the results in the CIE 1931 *Yxy* and CIE 1976 *L*a*b** color spaces, as recommended by the "Commission Internationale de l'Eclairage" (CIE).[44] The colors observed for each polymer are summarized in Table 3. Except PEDOP, which changes from red to light sky blue upon oxidation, the other PXDOPs switch from orange to gray/blue with a brown intermediate color.

Table 3. Colors Observed in PXDOPs with Coordinates Expressed in the CIE 1976 *L*a*b Space**

polymer	neutral	intermediate	doped
PEDOP	$L = 50$, $a = 77$, $b = 20$ red	none	$L = 96$, $a = -3$, $b = 0$ light sky blue
PProDOP	$L = 79$, $a = 31$, $b = 93$ orange	$L = 62$, $a = 11$, $b = 23$ brown	$L = 83$, $a = 0$, $b = 1$ light gray/blue
PProDOP−CH_3	$L = 76$, $a = 47$, $b = 85$ orange	$L = 59$, $a = 28$, $b = 23$ brown/red	$L = 77$, $a = -3$, $b = -8$ light blue
PProDOP−$(CH_3)_2$	$L = 76$, $a = 57$, $b = 70$ orange	$L = 59$, $a = 39$, $b = 25$ red/brown	$L = 81$, $a = -2$, $b = -5$ light blue
PBuDOP	$L = 72$, $a = 47$, $b = 69$ orange	$L = 60$, $a = 26$, $b = 19$ orange/brown	$L = 78$, $a = -2$, $b = -3$ light blue/gray

The luminance, which represents the brightness of a color, is very informative since with only one value, it provides information about the perceived transparency of a sample over the entire visible range of light. Instead of *Y*, it is usually more convenient to express the luminance as %*Y*, which corresponds to the luminance through the sample relative to the luminance of the light source. It should be pointed out that %*Y* is different from %*T* because it takes into account the light sensitivity of the human eye, which is not constant over the entire visible range.[45] In fact, the human eye perceives brightness with a maximum sensitivity at 550 nm (yellow light), while under 480 nm or above 650 nm, the sensitivity is 10 times less. The relative luminance (%*Y*) results for 1 μm thick PEDOP and PProDOP films are presented in parts A and B of Figure 10, respectively. In PEDOP, the relative luminance increases upon oxidation from 11% to 56%. This is expected as the absorbance of the $\pi-\pi^*$ transition located at 537 nm in the visible spectrum is depleted while the oscillator strength is shifted to the NIR. At potentials greater than −0.1 V vs Fc/Fc^+, the tail of the NIR band that extends into the visible region decreases in intensity, leading to an increase in the luminance of the material. This bleaching at high doping levels has already been observed in the PXDOTs.[46] Although the spectroelectrochemistry of the other PXDOPs, as exemplified by PProDOP (Figure 7B), suggests a similar behavior, it can be seen in Figure 10B that this is not the case. PProDOP has a relatively high luminance value in the neutral state (60%) and reaches 70% in the fully doped state. Moreover, at a potential of about −0.5 V vs Fc/Fc^+, a dark intermediate state can be seen with a relative luminance of 33%. This intermediate state comes from a rapid increase in absorbance due the tail of the growing NIR band, coupled with substantial residual absorbance of the $\pi-\pi^*$ transition. This was illustrated earlier in the transmittance results presented in Figure 8. While this effect is also observed in PEDOP spectroelectrochemistry, the lower value of the relative luminance in neutral PEDOP is explained by the fact that PEDOP is red, a color which is perceived darker by the human eye.

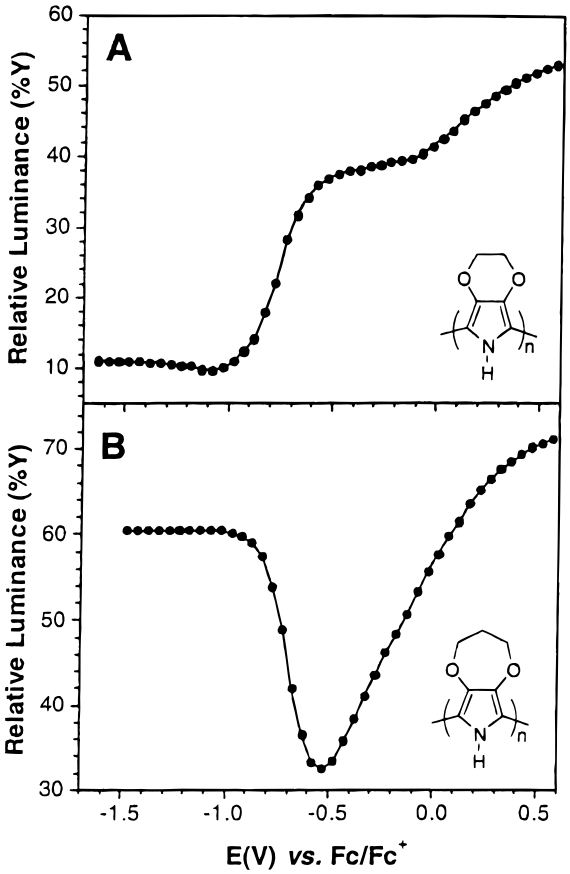

Figure 10. (A) Relative luminance of 1 μm thick PEDOP film as calculated from the *Yxy* coordinates as a function of the potential applied vs Fc/Fc^+. (B) Relative luminance of 1 μm thick PProDOP film as calculated from the *Yxy* coordinates as a function of the potential applied vs Fc/Fc^+.

Conclusion. In summary, a series of new poly(3,4-alkylenedioxypyrrole)s (PXDOPs) have been prepared which show some of the lowest oxidation potentials (if not the lowest) for any conducting polymer reported to date. This enhances the stability of the doped state to ambient reduction when compared to regular polypyrrole. The PXDOPs show outstanding electrochemical stability and are able to withstand potentials up to 2 V above their half-wave potential prior to overoxidizing. As electrochromic materials, the poly(3,4-alkylenedioxypyrrole)s can switch many thousands of times between their red or orange neutral state and a light blue/gray doped state with a high degree of contrast in less than 200 ms. To the best of our knowledge, no other polymers exhibit this extreme color change. Moreover, the low oxidation potentials of these polymers introduce a new dimension in electrochromic device construction in that they can be used in a very wide potential window (at least −1.5 to +1.3 V), thus making them compatible with numerous polymers in dual polymer devices. Another important feature of these new compounds is the ease with which they can be derivatized. The introduction of long alkyl chains on the alkylenedioxy ring provides a promising route toward the production of soluble conducting polymers, while N-substitution provides a means to control the electronic and optical properties through steric interactions.[47]

Experimental Section

All chemicals were purchased from Aldrich Chemical. Propylene carbonate (99.8%, anhydrous) was distilled over calcium hydride before use. ^1H NMR spectra were recorded on a

Tecmag QE 300 FT-NMR spectrometer at 300 MHz. Elemental analyses were carried out by Robertson Microanalytical Laboratories, Inc. High-resolution mass spectrometry (HRMS) was performed by the Spectroscopic Services Department of the Chemistry Department of University of Florida.

Electropolymerization was carried out with an EG&G Princeton Applied Research model 273 potentiostat/galvanostat employing a platinum button working electrode (diameter, 1.6 mm; area, 0.02 cm^2), a platimum wire counter electrode, and a silver wire pseudoreference. The electrolyte used was 0.1 M lithium perchlorate in propylene carbonate. The pseudoreference was calibrated externally using a 5 mM solution of ferrocene (Fc/Fc^+) in the electrolyte ($E_{1/2}(Fc/Fc^+) = +0.13$ V vs silver wire in 0.1 M $LiClO_4$/PC). Note 1.0 V vs $Fc/Fc^+ = 1.07$ V vs $Ag/Ag^+ = 0.7$ V vs SCE.[48] All potentials are reported versus Fc/Fc^+ as recommended by the IUPAC.[49] Electrodepositions were carried out from a 10 mM solution of monomer in 0.1 M electrolyte at a scan rate of 20 mV/s for 20 cycles.

Cyclic voltammetry was carried out using the same electrode setup using monomer-free electrolyte. The electrolyte used was 0.1 M lithium perchlorate in propylene carbonate. All potentials are reported versus Fc/Fc^+. The default scan rate was set to 20 mV/s for cyclic voltammetry. Corrware II software from Scribner Associates was used for data acquisition and control of the potentiostat.

Spectroelectrochemical results were recorded on a Varian Cary 5E UV−vis−NIR spectrophotometer at a scan rate of 600 nm/min. A three-electrode cell assembly was used where the working electrode was an ITO-coated glass (7 × 50 × 0.6 mm, 10 Ω/□, Delta Technologies Inc.); the counter was a platinum wire along with a 10 mM $Ag/AgNO_3$ reference electrode. The potentials were applied using the same EG&G potentiostat as previously described and the data recorded with Corrware II software for electrochemical data and with the Varian Cary Win-UV for spectral data.

Colorimetry measurements were obtained using a Minolta CS-100 chroma meter and CIE recommended normal/normal (0/0) illuminating/viewing geometry for transmittance measurements.[45] A similar three-electrode cell as for spectroelectrochemistry was employed. The sample was illuminated from behind by a D50 (5000 K) light source in a light booth designed to exclude external light. The color coordinates are expressed in the CIE 1931 Yxy color space where the Y value is a measure of the luminance in Cd/m^2. The relative luminance, expressed in percent, was determined relative to the background light source. Note that the relative luminance is frequently reported as opposed to the absolute value of luminance as it gives a more meaningful value.[50]

Polymer films for spectroscopy and conductivity studies were prepared by galvanostatic deposition on ITO (R_s 10 Ω/□). ITO supported films were grown in a propylene carbonate solution at 0.1 mA for varying times. Free-standing films for conductivity studies were prepared by long-term growth (24 h) at low current densities (ca. 0.04 mA/cm^2) on ITO or glassy carbon at −7 °C and monomer/electrolyte concentrations of 0.6 M each. The films were washed in acetonitrile, dried under vacuum for 24 h, and then peeled from the working electrode.

Film thicknesses were measured using a Sloan Dektak 3030 profilometer. Films were scored with a piece of glass, and a total of 500 μm spanning the score was measured using a stylus force of 30 mg and a vertical resolution of 1 Å. Thickness was measured as the difference between the valley and the average surface height.

X-ray Crystallography, Data Collection, Structure Solution, and Refinement. Data were collected at 173 K on a Siemens SMART PLATFORM equipped with A CCD area detector and a graphite monochromator utilizing Mo Kα radiation ($\lambda = 0.710$ 73 Å). Cell parameters for each structure were refined using up to 8192 reflections, and a hemisphere of data (1381 frames) was collected using the ω-scan method (0.3° frame width). The first 50 frames were remeasured at the end of data collection to monitor instrument and crystal stability (maximum correction on I was < 1%). Absorption corrections by integration were applied on the basis of measured indexed crystal faces.

The structure was solved by the Direct Methods in *SHELXTL5* and refined using full-matrix least squares.[51] The non-H atoms were treated anisotropically, whereas the hydrogen atoms were calculated in ideal positions and were riding on their respective carbon atoms. A total of 83 parameters for EDOP were refined in the final cycle of refinement using 964 reflections with $I > 2\sigma(I)$ to yield R_1 and wR_2 of 4.08% and 10.15%, respectively. For ProDOP, a total of 91 parameters were refined in the final cycle of refinement using 1236 reflections with $I > 2\sigma(I)$ to yield R_1 and wR_2 of 3.80% and 9.22%, respectively. For BuDOP, a total of 101 parameters were refined in the final cycle of refinement using 1455 reflections with $I > 2\sigma(I)$ to yield R_1 and wR_2 of 3.77% and 10.11%, respectively. Refinement was done using F^2. Basic X-ray crystallographic data are shown in Table 1. A more extensive listing of data is contained in the Supporting Information.

General Synthesis of 3,4-Alkylenedioxypyrroles (6a−e): The 3,4-alkylenedioxypyrroles monomers were synthesized by a modification of a procedure developed by Merz and coworkers.[33] A mixture of dimethyl *N*-benzyl-3,4-dihydroxypyrrole-2,5-dicarboxylate (0.1 mol), alkyl dibromide or alkyl dimesylate (0.1 mol), and K_2CO_3 (0.5 mol) in dry DMF was stirred for 12 h under argon at 105−110 °C. After cooling to room temperature, the reaction mixture was poured onto ice−water. The crude product was collected by suction filtration and purified by recrystallization in methanol, yielding compound **3a** as colorless crystals (55−65%); mp 145−146 °C. ^{1}H NMR (300 MHz, $CDCl_3$): δ 7.25−7.15 (m, 3H), 6.90−6.98 (m, 2H), 5.99 (s, 2H), 4.33 (s, 4H), 3.80 (s, 6H). **3b**: pale yellow crystals (75−80%); mp 150−151 °C. ^{1}H NMR (300 MHz, $CDCl_3$): δ 7.25−7.15 (m, 3H), 6.99−6.90 (m, 2H), 5.95 (s, 2H), 4.23 (t, $J = 5.5$ Hz, 4H), 3.80 (s, 6H), 2.26 (quintet, $J = 5.5$ Hz, 2H). **3c**: colorless crystals (38−45%); mp 101−102 °C. ^{1}H NMR (300 MHz, $CDCl_3$): δ 7.25−7.15 (m, 3H), 6.99−6.90 (m, 2H), 5.97 (s, 2H), 4.40−4.35 (m, 4H), 3.82 (s, 6H), 1.96−1.94 (m, 4H). **3d**: colorless crystals (76−80%); mp 108−109 °C. ^{1}H NMR (300 MHz, $CDCl_3$): δ 7.25−7.15 (m, 3H), 6.99−6.90 (m, 2H), 5.95 (s, 2H), 4.23 (dd, $J = 12.1$, 3.8 Hz, 2H), 3.88 (dd, $J = 11.5$, 6.6 Hz, 2H), 3.82 (s, 6H), 2.46 (m, 1H), 1.07 (d, $J = 7.2$ Hz, 3H). **3e** (the ester group equals to ethyl ester): colorless crystals (20−23%); mp 88−89 °C. ^{1}H NMR (300 MHz, $CDCl_3$): δ 7.25−7.15 (m, 3H), 6.90−6.98 (m, 2H), 5.92 (s, 2H), 4.25 (q, $J = 7.8$ Hz, 4H), 3.80 (s, 4H), 1.26 (t, $J = 7.8$ Hz, 6H), 1.08 (s, 6H).

For the removal of the benzyl group (deprotection of the nitrogen atom in the pyrrole ring), methods i and ii were used. Method i is a catalytic transfer hydrogenation (**3a**, **3b**, and **3c**) whereas method ii is a solvolytic debenzylation (**3d** and **3e**). To the solution of **3a**−**c** in acetic acid was carefully added 10% palladium on activated carbon (15−20 mol %). After stirring for 5 min, the reaction mixture was thoroughly flushed with hydrogen using a balloon. A hydrogen balloon (thick-wall, natural latex rubber, from Aldrich) was then fitted to the reaction vessel. The reaction mixture was stirred vigorously for 48 h at 70 °C. (The replacement by a new hydrogen balloon at the middle of the entire reaction time is necessary.) After completion of the reaction, the catalyst was filtered off through a Celite bedded funnel while the mixture was still hot to prevent crystallization of the substituted heterocycle. Removal of acetic acid by rotary evaporation and then drying under high vacuum afforded the crude crystalline products, **4a**−**c**. The crude compound was usually used in the next step without further purification. For solvolytic debenzylation, the reaction mixture of **3d**−**e**, 98% sulfuric acid (10 mol %), and anisole (1.5 equiv) in trifluoroacetic acid was stirred for 0.5 h at 90 °C. After cooling to room temperature, the solvent was removed by rotary evaporator and purified by column chromatography on silica gel using hexane/ethyl acetate (3:1) to provide **4d**−**e**.

Compounds **4a**−**e** were suspended in a 2.5 M aqueous NaOH solution and solublized with a small amount of ethanol. The reaction mixture was stirred for 6 h at 60−65 °C, cooled to room temperature, and subsequently extracted with ether

and the organic layer discarded. The basic aqueous layer was cooled in an ice bath and acidified to pH 2−3 by concentrated HCl. The diacids **5a**−**e** were obtained through filtration as a white solid. The diacids **5a**−**e** were pure enough to be used for next step. In a two-necked flask fitted with a reflux condenser connected to argon line, triethanolamine was added and heated to 180 °C. The diacids **5a**−**e** were added in one portion with vigorous stirring, and heating was maintained until CO_2 evolution ceased. The reaction mixture was poured into ice−water, and the aqueous solution was extracted with dichloromethane three times. The combined organic layers were dried over $MgSO_4$ and concentrated under reduced pressure to give a tan or brown solid. The crude product was purified by vacuum sublimation (0.01 mmHg) or recrystallization to give **6a**−**e** as colorless crystals.

3,4-Ethylenedioxypyrrole (EDOP, 6a): colorless crystals; mp 107−108 °C (from CH_2Cl_2/EtOAc/Hexane) [lit.[33] mp 106−107 °C]. ^{1}H NMR (300 MHz, $CDCl_3$): δ 7.06 (br, 1H), 6.21 (d, J = 3.0 Hz, 2H), 4.21 (S, 4H). UV−vis (H_2O): λ_{max} = 220, ϵ = 5700. MS (EI): m/z 125 (M^+, 100.0). HRMS (EI): m/z calcd for $C_6H_7NO_2$ 125.0476, obsd 125.0528. Anal. Calcd for $C_6H_7NO_2$: C, 57.59; H, 5.64; N, 11.19. Found: C, 57.71; H, 5.62; N, 11.19.

3,4-Propylenedioxypyrrole (ProDOP, 6b): colorless crystals; mp >180°C (decomposition) (from CH_2Cl_2/EtOAc/hexane). ^{1}H NMR (300 MHz, $CDCl_3$): δ 7.32 (br, 1H), 6.52 (d, J = 3.0 Hz, 2H), 4.01 (m, 4H), 2.16 (m, 2H). UV−vis (H_2O): λ_{max} = 209, ϵ = 6000. MS (EI): m/z 139 (M^+, 100.0). HRMS (EI) m/z calcd for $C_7H_9NO_2$ 139.0633, obsd 139.0644. Anal. Calcd for $C_7H_9NO_2$: C, 60.42; H, 6.52; N, 10.07. Found: C, 60.66; H, 6.50; N, 9.60.

3,4-Butylenedioxypyrrole (BuDOP, 6c): colorless crystals; mp 75−76 °C (from EtOAc/hexane). ^{1}H NMR (300 MHz, $CDCl_3$): δ 7.25 (br, 1H), 6.28 (d, J = 3.2 Hz, 2H), 4.23 (m, 4H), 1.97 (m, 4H). UV−vis (H_2O): λ_{max} = 210, ϵ = 5300. MS (EI): m/z 153 (M^+, 100.0). HRMS (EI) m/z calcd for $C_8H_{11}NO_2$ 153.0789, obsd 153.0805. Anal. Calcd for $C_8H_{11}NO_2$: C, 62.73; H, 7.24; N, 9.14. Found: C, 62.70; H, 7.10; N, 9.00.

3,4-Propylenedioxypyrrole-Me (ProDOP−CH_3, 6d): colorless crystals; mp 140−141 °C (from EtOAc/hexane). ^{1}H NMR (300 MHz, $CDCl_3$): δ 7.16 (br, 1H), 6.31 (d, J = 3.3 Hz, 2H), 4.03 (dd, J = 12.0, 2.7, 2H), 3.60 (dd, J = 11.6, 5.3, 2H), 2.29 (m, 1H), 0.99 (d, J = 7.1, 3H). UV−vis (H_2O): λ_{max} = 211, ϵ = 6200. MS (EI): m/z 153 (M^+, 100.0). HRMS (EI): m/z calcd for $C_8H_{11}NO_2$ 153.0789, obsd 153.0832. Anal. Calcd for $C_8H_{11}NO_2$: C, 62.73; H, 7.24; N, 9.14. Found: C, 62.69; H, 7.06; N, 8.99.

3,4-Propylenedioxypyrrole-Me_2 (ProDOP−$(CH_3)_2$, 6e): colorless crystals; mp 130−131°C (from EtOAc/hexane). ^{1}H NMR (300 MHz, $CDCl_3$): δ 7.05 (br, 1H), 6.30 (d, J = 3.0 Hz, 2H), 3.64 (S, 4H), 1.02 (s, 6H). UV−vis (H_2O): λ_{max} = 212, ϵ = 5900. MS (EI): m/z 167 (M^+, 100.0). HRMS (EI) m/z calcd for $C_9H_{13}NO_2$ 167.0946, obsd 167.0953. Anal. Calcd for $C_9H_{13}NO_2$: C, 64.65; H, 7.84; N, 8.38. Found: C, 64.68; H, 7.57; N, 8.04.

Acknowledgment. We gratefully acknowledge support from the National Science Foundation (CHE 96-29854), the Air Force Office of Scientific Research (F49620-00-1-0047), the Naval Air Warfare Center, and the U.S. Army Research Office (DAAD19-99-1-0316). We also acknowledge the sponsors of the NSF REU program at the University of Florida and Scribner Associates' Corrware and Corrview Electrochemical Software package. Khalil A. Abboud acknowledges the National Science Foundation and the University of Florida for funding of the purchase of the X-ray equipment.

Supporting Information Available: Tables of full X-ray crystallographic data. This material is available free of charge via the Internet at http://pubs.acs.org.

References and Notes

(1) Deb, S. K. *Appl. Opt., Suppl.* **1969**, *3*, 192.
(2) Monk, P. M. S.; Mortimer, R. J.; Rosseinsky, D. R. *Electrochromism: Fundamentals and Applications;* VCH: Weinheim, 1995.
(3) Granqvist, C. G.; Azens, A.; Isidorsson, J.; Kharrazi, M.; Kullman, L.; Lindstroem, T.; Niklasson, G. A.; Ribbing, C.-G.; Roennow, D.; Stromme Mattsson, M.; Veszelei, M. *J. Non-Cryst. Solids* **1997**, *218*, 273.
(4) Monk, P. M. S. *J. Electroanal. Chem.* **1997**, *432*, 175.
(5) Bange, K. *Sol. Energy Mater. Sol. Cells* **1999**, *58*, 1.
(6) Granqvist, C. G.; Azens, A.; Hjelm, A.; Kullman, L.; Niklasson, G. A.; Ribbing, C.-G.; Roennow, D.; Stromme Mattsson, M.; Veszelei, M.; G. Vaivars *Sol. Energy* **1998**, *63*, 199.
(7) Agnihotry, S. A.; Pradeep; Sekhon, S. S. *Electrochim. Acta* **1999**, *44*, 3121.
(8) Rauh, R. D. *Electrochim. Acta* **1999**, *44*, 3165.
(9) Tracy, C. E.; Zhang, J.-G.; Benson, D. K.; Czanderna, A. W.; Deb, S. K. *Electrochim. Acta* **1999**, *44*, 3195.
(10) Pennisi, A.; Simone, F.; Barletta, G.; Di Marco, G.; Lanza, L. *Electrochim. Acta* **1999**, *44*, 3237.
(11) Meeker, D. L.; Mudigonda, D. S. K.; Osborn, J. M.; Loveday, D. C.; Ferraris, J. P. *Macromolecules* **1998**, *31*, 2943.
(12) Mudigonda, D. S. K.; Meeker, D. L.; Loveday, D. C.; Osborn, J. M.; Ferraris, J. P. *Polymer* **1999**, *40*, 3407.
(13) Brotherson, I. D.; Mudigonda, D. S. K.; Ocborn, J. M.; Belk, J.; Chen, J.; Loveday, D. C.; Boehme, J. L.; Ferraris, J. P.; Meeker, D. L. *Electrochim. Acta* **1999**, *44*, 2993.
(14) Byker, H. J. Gentex Corporation, US Patent No. 4902108.
(15) Mortimer, R. G. *Chem. Soc. Rev.* **1997**, *26*, 147.
(16) For an overview see: *Electrochim. Acta* **1999**, *44*.
(17) Mortimer, R. J. *Electrochim. Acta* **1999**, *44*, 2971.
(18) Mastrogostino, M. *Applications of Electroactive Polymers*; Scrosati, B., Ed.; Chapman and Hall: London, 1993.
(19) De Paoli, M.-A.; Casabollore-Miceli, G.; Girotto, E. M.; Gazotti, W. A. *Electrochim. Acta* **1999**, *44*, 2983.
(20) Sapp, S. A.; Sotzing, G. A.; Reynolds, J. R. *Chem. Mater.* **1998**, *10*, 2101.
(21) Kumar, A.; Welsh, D. M.; Morvant, M. C.; Piroux, F.; Abboud, K. A.; Reynolds, J. R. *Chem. Mater.* **1998**, *10*, 896.
(22) Skotheim, T. A.; Elsenbaumer, R. L.; Reynolds, J. R. *Handbook of Conducting Polymers*, 2nd ed.; Marcel Dekker: New York, 1998.
(23) Diaz, A. F.; Castillo, J. I.; Logan, J. A.; Lee, W.-Y. *J. Electroanal. Chem.* **1981**, *129*, 115.
(24) Heywang, G.; Jonas, F. *Adv. Mater.* **1992**, *4*, 116.
(25) Sotzing, G. A.; Reynolds, J. R.; Steel, P. J. *Chem. Mater.* **1996**, *8*, 882.
(26) Reynolds, J. R.; Ruiz, J.; Child, A.; Nayak, K.; Marynick, D. *Macromolecules* **1991**, *24*, 678.
(27) Ruiz, J.; Dharia, J.; Reynolds, J. R.; Buckley, L. *Macromolecules* **1992**, *25*, 849.
(28) Child, A.; Sankaran, B.; Larmat, F.; Reynolds, J. R. *Macromolecules* **1995**, *28*, 6571.
(29) Pfluger, P.; Street, G. B. *J. Chem. Phys.* **1984**, *80*, 544.
(30) Thomas, C. A.; Zong, K.; Schottland, P.; Reynolds, J. R. *Adv. Mater.* **2000**, *12*, 222.
(31) Pei, Q.; Zucharello, M.; Ahlskog, M.; Inganas, O. *Polymer* **1994**, *35*, 1347.
(32) Sankaran, B.; Reynolds, J. R. *Macromolecules* **1997**, *30*, 2582.
(33) Merz, A.; Schropp, R.; Dötterl, E. *Synthesis* **1995**, 795.
(34) Ouyang, J.; Li, Y. *Polymer* **1997**, *38*, 1971.
(35) Pernaut, J.-M.; Peres, R. C. D.; Julianio, V. F.; DePaoli, M. A. *J. Electroanal. Chem.* **1989**, *274*, 225.
(36) Salmon, M.; Diaz, A. F.; Logan, A. J.; Kroubni, M.; Bargon, J. *Mol. Cryst. Liq. Cryst.* **1982**, *83*, 265.
(37) Aleshin, A.; Kiebooms, R.; Menon, R.; Heeger, A. J. *Synth. Met.* **1997**, *90*, 61.
(38) Aleshin, A.; Kiebooms, R.; Menon, R.; Heeger, A. J. *Phys. Rev. B* **1997**, *56*, 3659.
(39) Chen, X. B.; Issi, J.-P.; Devaux, J.; Billaud, D. *J. Mater. Sci.* **1997**, *32*, 1515.
(40) Genies, E.; Pernaut, J.-M. *J. Electroanal. Chem.* **1985**, *191*, 111.
(41) Rughooputh, S. D. D. V.; Heeger, A. J.; Wudl, F. *J. Polym. Sci.* **1987**, *25*, 1071.
(42) Roncali, J. *Chem. Rev.* **1997**, *97*, 173.
(43) Bredas, J. L. *J. Chem. Phys.* **1985**, *82*, 3808.
(44) CIE: *Colorimetry* (Official Recommandations of the International Commission on Illumination), CIE Publication No. 15, Paris, 1971.
(45) Nassau, K. *Color for Science, Art and Technology*; Elsevier: Amsterdam, 1998.
(46) Thompson, B. C.; Schottland, P.; Zong, K.; Reynolds, J. R. *Chem. Mater.* **2000**, *12*, 1563.

(47) Zong, K.; Reynolds, J. R. *J. Org. Chem.*, in preparation.
(48) Bard, A. J.; Faulkner, L. R. *Electrochemical Methods, Fundamentals and Applications*; John Wiley & Sons: New York, 1980; p 701.
(49) Gritzner, G.; Kuta, G. *J. Pure Appl. Chem.* **1984**, *56*, 461.
(50) Overheim, R. D.; Wagner, D. L. *Light and Color*; John Wiley & Sons: New York, 1982; p 77.
(51) Sheldrick, G. M. *SHELXTL5*; Bruker-AXS: Madison, WI, 1998.

MA000490F